



## Article

# Sorption and Spatial Distribution of $^{137}\text{Cs}$ , $^{90}\text{Sr}$ and $^{241}\text{Am}$ on Mineral Phases of Fractured Rocks of Nizhnekansky Granitoid Massif

Anastasiya A. Rodionova <sup>1,2</sup>, Vladimir G. Petrov <sup>1,\*</sup> , Irina E. Vlasova <sup>1</sup> , Konstantin B. Rozov <sup>3</sup>, Iurii M. Nevolin <sup>1,4</sup>, Vasiliy O. Yapaskurt <sup>5</sup>, Vyacheslav G. Rumynin <sup>3</sup> and Stepan N. Kalmykov <sup>1</sup>

<sup>1</sup> Department of Chemistry, Lomonosov Moscow State University, Leninskie Gory 1 bld. 3, 119991 Moscow, Russia

<sup>2</sup> Vernadsky Institute of Geochemistry and Analytical Chemistry of Russian Academy of Sciences, Kosygin st. 19, 119991 Moscow, Russia

<sup>3</sup> Institute of Environmental Geology, Russian Academy of Sciences, Sredniy Ave., 41, 199004 St. Petersburg, Russia

<sup>4</sup> Frumkin Institute of Physical Chemistry and Electrochemistry, Russian Academy of Sciences, Leninsky Prospect 31 bld. 4, 119071 Moscow, Russia

<sup>5</sup> Department of Geology, Lomonosov Moscow State University, Leninskie Gory 1, 119991 Moscow, Russia

\* Correspondence: vladimir.g.petrov@gmail.com



**Citation:** Rodionova, A.A.; Petrov, V.G.; Vlasova, I.E.; Rozov, K.B.; Nevolin, I.M.; Yapaskurt, V.O.; Rumynin, V.G.; Kalmykov, S.N.

Sorption and Spatial Distribution of  $^{137}\text{Cs}$ ,  $^{90}\text{Sr}$  and  $^{241}\text{Am}$  on Mineral Phases of Fractured Rocks of Nizhnekansky Granitoid Massif. *Energies* **2022**, *15*, 7440. <https://doi.org/10.3390/en15197440>

Academic Editor: Antonio Zuorro

Received: 26 August 2022

Accepted: 5 October 2022

Published: 10 October 2022

**Publisher's Note:** MDPI stays neutral with regard to jurisdictional claims in published maps and institutional affiliations.



**Copyright:** © 2022 by the authors. Licensee MDPI, Basel, Switzerland. This article is an open access article distributed under the terms and conditions of the Creative Commons Attribution (CC BY) license (<https://creativecommons.org/licenses/by/4.0/>).

**Abstract:** The sorption behavior and spatial microdistribution of Cs-137, Sr-90 and Am-241 onto the surface of a fractured rock sample from the R-11 borehole of the exocontact zone of the Nizhnekansky granitoid massif were studied. The sorption efficiency of the fractured sample increases in the row of  $\text{Sr} < \text{Cs} < \text{Am}$ , where americium is the most retained radionuclide. Based on the image processing of radiograms and scanning electron microscopy data, the mineral relative sorption efficiency (RSE) values were determined to quantify the contribution of the mineral phases of the fractured sample to radionuclide retention. It was established that cesium and strontium are predominantly retained in cracks filled with secondary mineral chlorite. Zeolite is a less effective sorbent with respect to cesium and strontium. Americium sorption is uniform over the whole surface of the fractured sample, with close RSE values for all mineral phases (RSE ~1). The behavior of cesium in heterogeneous and monomineral systems of crushed mineral phases of quartz, biotite and zeolite NaA imitating minerals of the fractured rock sample R-11 was determined. It was shown that the fraction of the sorbed cesium in a heterogeneous system of two mineral phases—biotite and quartz—was larger than the sum of sorption values for the same separated mineral phases. Based on the models of radionuclide sorption on illite–smectite minerals, it was able to estimate the depth of the penetration of solution into the fractured rock sample R-11. The variations of penetration depths for solutions of specific radionuclide into the fractured rock sample were established.

**Keywords:** sorption; spatial microdistribution of radionuclides; digital autoradiography; fractured rock sample; Nizhnekansky granitoid massif; relative sorption efficiency of minerals; models of radionuclide sorption

## 1. Introduction

The removal of radioactive waste from the human environment is essential for the future of the nuclear industry around the world. High-level radioactive waste (HLW), as well as intermediate-level radioactive waste (ILW) containing long-lived radionuclides with a radiobiological hazard period of more than  $10^4$ – $10^5$  years, poses a particular environmental problem [1]. According to the generally accepted concept, the most efficient way to manage HLW and long-lived ILW is to disposal of them in deep geological formations; thus, at present, the worldwide search for sites with different geology suitable for the creation of deep repositories is active [2–4]. In many countries, such as Switzerland, Finland, Sweden,

Japan, Great Britain and Russia, crystalline rocks are considered one of the geological formations suitable for waste disposal [5–9]. The crystalline rocks considered in Russia are represented by the Precambrian gneiss strata, which are located on the western boundary of the Nizhnekansky granitoid massif (Krasnoyarsk region, the “Yeniseisky” site), where an underground research laboratory is currently being constructed [10,11].

One of the most significant factors affecting the safety of radioactive waste disposal in crystalline rocks is the presence of fractured zones in them, which influence the stability of the rocks, the intensity of deformation and the water permeability [12]. It is assumed that cracks are both the main migration pathways for radionuclides and their retention in the porous rock matrix made by finely dispersed mineral phases [13–15]. The main mechanism of radionuclide retention during transportation through rock is the sorption on the surface of the mineral grains of cracks. It was noted that secondary minerals filling the cracks play an important role in retarding the transfer of radionuclides, as they have good sorption properties [16,17].

The sorption properties of the crushed samples of the fracture filler material of the Nizhnekansky granitoid massif with respect to Cs, Sr, Se, Tc and Eu were studied in the work [18]. It was established that the highest sorption activity towards Cs, Eu and Pu demonstrate rocks from the contact zone of gneisses and dolerites, with distribution coefficients about  $10^3 \text{ mL} \cdot \text{g}^{-1}$ . Such a high sorption capacity of these rock samples is due to the presence of chlorite, clay minerals and calcite in the material filler of the cracks. It was shown by digital radiography of a sample from the Toki Granite with fractured zones that alpha-emitting nuclides (uranium and thorium) are localized in the accessory minerals (apatite, orthite and zircon) in the zone of chloritized biotite, as well as in the clay matrix of the host rock [19]. Canadian researchers studied the sorption of Cs, Sr, Ce, Am, Se and Tc on thin sections of gabbroic rocks by digital radiography [20]. As a result, the authors noted that for almost all the studied radionuclides, the sorption on the secondary mineral assemblages was significantly higher than on the primary rock-forming minerals. Olivine, serpentine and chlorite showed a high sorption capacity in relation to selenium. Kaolinite, laumontite and sericite were effective for the sorption of Sr, Cs, Am and Se. Strontium sorbed on epidote as well. Magnetite was the only rock-forming mineral that sorbed technetium.

Thus, while studying radionuclide migration in conditions of underground disposal, it is necessary to take into account the mineral filling of fracture zones, as radionuclide localization mainly occurs in a specific mineral phase or mineral group. At the same time, the most effective sorbing mineral phases, taking into account the heterogeneity of the system, were established only in terms of the qualitative assessment so far, which makes it difficult to carry out modeling of the radionuclide migration.

This work is directed to study the microdistribution of radionuclides on the minerals of the rocks of the Nizhnekansky granitoid massif of the “Yeniseisky” site, taking into account the fractured zones, and to assess the contribution of mineral phases of the fractured zones in the sorption of cesium, strontium and americium by determining the quantitative parameters of the relative sorption efficiency [21]. To prove the parameters of the relative sorption efficiency obtained for the whole rock fractured sample, the sorption of cesium on crushed mineral phases simulating the minerals of the sample under study was also investigated in heterogeneous and monomineral systems.

To numerically reproduce the experimental data, sorption modeling was carried out. As a result, it was possible to estimate the depth of the penetration of radioactive aqueous solutions into the surface of the polished rock sample.

## 2. Materials and Methods

### 2.1. Characterization of the Whole Fractured Sample and Samples of Mineral Phases

To study radionuclide microdistribution on the rock surface, a core sample was taken from borehole R-11 of the “Yeniseisky” site of the Nizhnekansky granitoid massif exocontact zone at a depth of 249 m. The rock sample R-11 has a very complex heterogeneous

composition and belongs to the hydrothermally altered metasomatized gneisses, with the presence of calcite and zeolite veins. The choice of this rock sample was guided by the presence of fractured zones, which can play a main role in the migration and retention of radionuclides. The core, 6.5 cm in diameter, was cut into 6 mm thick discs (Figure 1). To avoid destroying the sample, the core was soaked in an ethyl cyanoacrylate glue, upon which sorption of the radionuclides under study was negligible. The disks were polished on one side for sorption studies and further radiography. The polished surface area of each disk averaged 32 cm<sup>2</sup>.

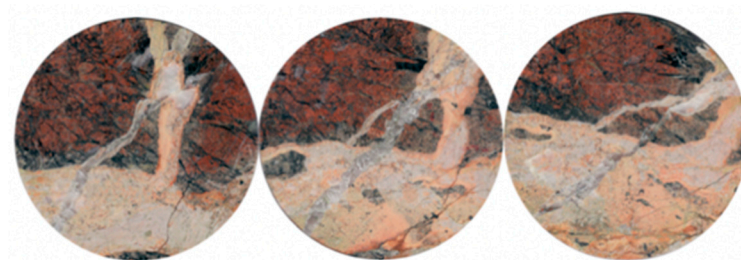


**Figure 1.** Discs of core sample from borehole R-11 from the depth of 249 m of the “Yeniseisky” site.

Sorption experiments were also performed on crushed monomineral phases, imitating the most effective sorbing phases of the fractured rock sample R-11. Further mineral analogues were chosen: MIN-U-SIL (SiO<sub>2</sub>) as a quartz imitator, biotite (K(Mg, Fe)<sub>3</sub>[Si<sub>3</sub>AlO<sub>10</sub>][OH, F]<sub>2</sub>) as a chlorite imitator and zeolite NaA (Na<sub>12</sub>[Al<sub>12</sub>Si<sub>22</sub>O<sub>48</sub>] 27H<sub>2</sub>O) as a zeolite (shabasite) imitator. Biotite, like chlorite, belongs to the phyllosilicates, which contain iron and magnesium, so they can be considered analogues. Values of the specific surface areas of the minerals were 0.4, 4.9 and 11.7 m<sup>2</sup> g<sup>−1</sup>, respectively. The grain size of the represented mineral phases was less than 0.1 mm.

## 2.2. Characterization of the Model Water Solution

Solutions simulating the underground natural water of the “Yeniseisky” site [18] and containing one of the studied radionuclides (Cs-137, Sr-90 or Am-241) were prepared for sorption experiments, both on the whole fractured sample R-11 and on the crushed samples of mineral phases. The radionuclide concentration in the solution without carriers was 10<sup>−9</sup> mol L<sup>−1</sup>, that corresponds to the initial activity of Cs-137, Sr-90 or Am-241 in solution 430, 285, 15 Bq mL<sup>−1</sup>, respectively. Values of the pH of the prepared solutions were 7–8. The main composition of the model water solution was confirmed by atomic emission spectrometry and is given in Table 1.

**Table 1.** Composition of the model water solution.

| Component                     | Concentration, mg L <sup>−1</sup> |
|-------------------------------|-----------------------------------|
| Cl <sup>−</sup>               | 36                                |
| SO <sub>4</sub> <sup>2−</sup> | 15                                |
| CO <sub>3</sub> <sup>2−</sup> | 18                                |
| HCO <sub>3</sub> <sup>−</sup> | 79                                |
| Na <sup>+</sup>               | 32.6                              |
| K <sup>+</sup>                | 3.9                               |
| Mg <sup>2+</sup>              | 10.2                              |
| Ca <sup>2+</sup>              | 18.5                              |

## 2.3. Conditions for Sorption Experiments on the Discs of Sample R-11

The sorption experiments were carried out in plastic vessels, with a liquid/solid ratio of 1 mL cm<sup>−2</sup>. The samples were placed horizontally on plastic supports so that the surface in contact with the solution was facing the bottom to exclude precipitation/co-precipitation processes (Figure S1). The walls of the discs were covered with thermal glue to prevent

sorption on them. The sorption on the materials of the plastic vessels as well as on the thermal glue was negligible. Before the beginning of experiment, the polished surfaces of the disks were kept in the model water solution for a week. The sorption was carried out under static conditions for the time necessary for the establishment of sorption equilibrium. After equilibrium was established, the disks were removed from the solution and rinsed with deionized water to exclude precipitation/co-precipitation effects. The concentration of radionuclides Cs-137 and Sr-90 in the solutions was determined by liquid scintillation counting (LSC) (Tri-Carb 2810 TR, Perkin Elmer, Waltham, MA, USA). The concentration of Am-241 in the solution was determined by gamma spectrometry using gamma spectrometer with a high-purity germanium detector GR 3818 (Canberra Inc, Meriden, CT, USA) and confirmed by LSC.

#### *2.4. Conditions for Sorption Experiments on Crushed Mineral Phases*

The sorption properties of the individual mineral phases of biotite, zeolite NaA and quartz were studied in relation to Cs-137. The experiments were carried out in plastic containers. There were two types of experiments: the sorption of cesium on individual minerals in separated containers and the sorption of cesium on individual minerals in the same container (competitive sorption). In order to ensure a reliable separation of the mineral phases, dialysis bags were used (Figure S2).

The mass of mineral phases was calculated on the basis of the fraction of the minerals' areas: chlorite corresponding to biotite, shabasite (zeolite) corresponding to zeolite NaA and quartz occupied on the surface of the whole disk (1) of sample R-11, and the depth of aqueous solution penetration 0.1 mm, determined from model calculations (Section 3.5.1). The liquid/solid ratio for each mineral in both systems was  $350 \text{ mL g}^{-1}$ , which was also chosen based on previous sorption experiments on the sample R-11. The sorption was carried out under static conditions for the time necessary to establish sorption equilibrium. The concentration of cesium in the solutions was monitored by the LSC method. After equilibrium was established, the dialysis bags were removed from the solutions and centrifuged at 5000 rpm to separate the liquid phase. The remaining solid mineral phases in the dialysis bags were dried at room temperature and then measured by gamma spectrometry to determine the amount of sorbed cesium.

#### *2.5. Determination of Mineral Phases in Sample R-11 (SEM-EDX, Micro XRF)*

The mineral composition of sample R-11 was studied using a scanning electron microscope with a thermionic tungsten cathode (JSM-6480LV, JEOL, Tokyo, Japan). The chemical composition of rock-forming minerals was analyzed using an electron probe method, utilizing an energy-dispersive spectrometer (X-Max-50, Oxford Instrument, Oxford, UK). Based on the energy-dispersive spectra it was possible to identify each mineral (mineral grains) separately using mineralogical databases. The distribution of mineral grains on each of the disks was established by micron resolution X-ray fluorescence spectrometry, micro XRF (Tornado M4+, Bruker, Bremen, Germany). The elemental maps for each of the studied discs were obtained.

#### *2.6. Determination of the Proportion of the Area Occupied by a Single Mineral Phase in the Sample R-11*

In order to quantify the mineral content on the surface of the sample discs under study, the ENVI (L3Harris Geospatial, Boulder, CO, USA) image processing program was used [22]. This program allows one to determine the proportion of the area occupied by a single mineral phase on the disc surface by processing its optical images with the already known mineral phases established by the SEM-EDX method.

#### *2.7. Digital Radiography Method*

The microdistribution of sorbed radionuclides over the disc surface of sample R-11 was investigated by digital autoradiography (DAR) using the Cyclone Storage System

(PerkinElmer, Waltham, MA, USA). The DAR system is based on the use of storage phosphor screens (Imaging Plates). DAR is one of the most sensitive methods to study the distribution of radionuclide microconcentrations in solid samples and tissues [23]. The digital radiography system is equipped with OptiQuant software, which allows obtaining black-and-white radiograms, showing the radionuclide microdistribution on the surface of sample discs. The exposure time for the discs of sample R-11 with sorbed Cs-137, Sr-90 and Am-241 varied from 6 h to 3–4 days. To analyze the radiograms according to the method [24], they were processed using the ImageJ (1.52 k, National Institutes of Health, Bethesda, MD, USA) program [25]. This program allows the conversion of black-and-white images to 16-color images. This conversion is based on the subdivision of the whole PSL intensity range into 16 subranges and the designation of each range with a definite color.

## 2.8. Determination of Sorption Parameters (the Degree of Sorption, Distribution Coefficients, Relative Sorption Efficiency)

The sorption value of each radionuclide was calculated based on the following ratio:

$$R(\%) = \frac{I_0 - I_t}{I_0} \times 100, \quad (1)$$

where  $I_0$  is the count rate (counts per minute, cpm) of the radionuclide in the initial solution;  $I_t$  is the count rate (cpm) of the radionuclide in the solution at time  $t$ .

The surface distribution coefficient of radionuclides ( $K_a$ ) was calculated for the surface area of the discs of the sample R-11 directly in contact with the solution, based on the following equation:

$$K_a \left( \text{mL cm}^{-2} \right) = \frac{I_0 - I_\infty}{I_\infty} \times \frac{V}{S}, \quad (2)$$

where  $I_0$  (cpm) is the count rate of the radionuclide in the initial solution;  $I_\infty$  (cpm) is the count rate of the radionuclide in the solution at the moment of system equilibrium;  $V$  (mL) is the solution volume;  $S$  (cm<sup>2</sup>) is the surface area of the disk contacting the solution.

The distribution coefficients ( $K_d$ ) of cesium on the mineral phases of quartz, zeolite NaA and biotite were determined as a result of monomineral experiments using dialysis bags (Equation (3)).

$$K_d \left( \text{mL g}^{-1} \right) = \frac{A_s}{A_\infty} \times \frac{V}{m}, \quad (3)$$

where  $A_s$  (Bq) is the activity of cesium on the sorbent;  $A_\infty$  (Bq) is the activity of cesium in the solution at the moment of system equilibrium;  $V$  (mL) is the volume of the solution;  $m$  (g) is the mass of the mineral sample in contact with the solution.

The parameter of the relative sorption efficiency (RSE) for minerals was determined based on previously developed methods [21,24] that are based on the comparison of radiogram images showing the microdistribution of radionuclides on the surface rock sample with SEM images informing about the mineral composition of the sample surface. The RSE was determined using the following relationship:

$$\text{RSE}_{i,j} = \frac{I_{i,j}/I_{j,0}}{S_i/S_0}, \quad (4)$$

where  $\text{RSE}_{i,j}$  is the relative sorption efficiency of the mineral phase  $i$  towards radionuclide  $j$ ;  $I_{i,j}$  is the intensity of luminescence on the radiogram attributed to radionuclide  $j$  sorbed onto the mineral phase  $i$ ;  $I_{j,0}$  is the intensity of luminescence on the radiogram attributed to radionuclide  $j$  sorbed onto the whole surface of a rock sample;  $S_i$  is the surface area of the mineral phase  $i$ ;  $S_0$  is the whole surface area of a rock sample.



The RSE parameter was also determined in the case of cesium sorption on individual mineral phases of the heterogeneous systems quartz–biotite, quartz–zeolite NaA, based on the following equation:

$$RSE_{i,Cs} = \frac{A_{i,Cs} / A_{i+j,Cs}}{S_{si} \times m_i / (S_{si} \times m_i + S_{sj} \times m_j)}, \quad (5)$$

where  $A_{i,Cs}$  (Bq) is the activity of sorbed cesium on mineral phase  $i$ ;  $A_{i+j,Cs}$  (Bq) is the total activity of sorbed cesium on minerals  $i$  and  $j$  of the two-component system;  $S_{si}$  and  $S_{sj}$  ( $\text{m}^2 \text{g}^{-1}$ ) are the specific surfaces of mineral phase  $i$  and  $j$ , respectively;  $m_i$  and  $m_j$  are the mass (g) of mineral phases  $i$  and  $j$ , respectively.

### 2.9. Modeling of Radionuclides Sorption

The sorption of Cs-137, Sr-90 and Am-241 on the polished sample R-11 was simulated using the data on the mineral composition and the composition of natural groundwater (depth 249 m). The PHREEQC software [26] was used to model the sorption equilibrium between the solution and the rock surface.

## 3. Results

### 3.1. Characterization of Rock Fractured Sample R-11

It was established that the whole rock sample R-11 includes various minerals: phyllosilicates (chlorite), sorosilicates (epidote), tectosilicates (feldspars, zeolite, quartz), oxides (rutile) and carbonates (calcite). The elemental composition of the main mineral phases of sample R-11 according to SEM-EDX analysis is given in Table S1. The mineral composition of sample R-11 was proved by results of spatial distribution of the minerals on the discs (microelement mapping, micro XRF). Maps of one of the studied sample discs (Figure 1) with defining elements for each mineral phase were allocated (Table S2).

To determine the proportion of the area occupied by an individual mineral phase on the disc surface, the optical images of the disc surface were treated using the ENVI program. As a result, color images were obtained for each disc, where each color corresponds to an individual mineral phase or stable association of mineral phases (Figure 2). The values of the mineral phase percentage on the surface of the discs were obtained (Table 2). In the three discs considered, the percentages of the areas of the mineral phases and the mineral associations varied as follows: quartz (11–15%), calcite (10–17%), chlorite (7–10%) and zeolite (13–30%); K-feldspar/quartz mineral association (20–25%) and quartz/K(Na)-feldspars association (15–32%).

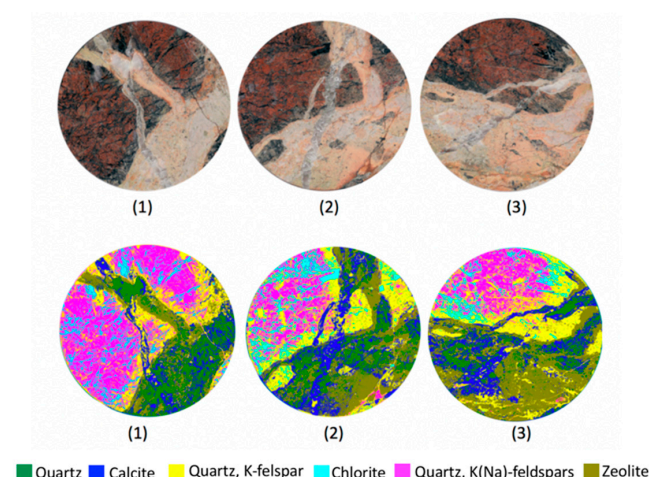


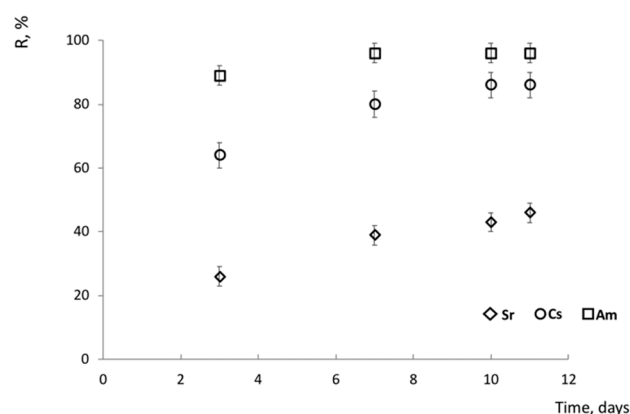
**Figure 2.** Optical images of three discs of the core sample R-11 (**top**); the same images treated in the ENVI program (**bottom**). Numbers in parentheses indicate disc titles.

**Table 2.** Determination of the part of the area occupied by individual mineral phases on the surface of discs of the R-11 sample using the ENVI program.

| Minerals                       | Quartz | Quartz,<br>K(Na)-Feldspars | Quartz,<br>K-Feldspars | Zeolite | Calcite | Chlorite |
|--------------------------------|--------|----------------------------|------------------------|---------|---------|----------|
| Disc (1)                       |        |                            |                        |         |         |          |
| Part of area, %                | 15.2   | 31.9                       | 19.8                   | 12.8    | 10.0    | 10.3     |
| Occupied area, cm <sup>2</sup> | 4.9    | 10.2                       | 6.4                    | 4.1     | 3.2     | 3.3      |
| Disk (2)                       |        |                            |                        |         |         |          |
| Part of area, %                | 13.7   | 13.8                       | 25.0                   | 20.3    | 16.9    | 10.4     |
| Occupied area, cm <sup>2</sup> | 4.4    | 4.5                        | 8.0                    | 6.5     | 5.4     | 3.3      |
| Disk (3)                       |        |                            |                        |         |         |          |
| Part of area, %                | 10.9   | 14.6                       | 24.0                   | 29.0    | 15.0    | 6.5      |
| Occupied area, cm <sup>2</sup> | 3.5    | 4.7                        | 7.7                    | 9.4     | 4.8     | 2.1      |

### 3.2. Sorption Experiments on Polished Discs of Sample R-11

As a result of the static sorption experiments on the discs of the sample R-11, kinetic sorption curves were obtained (Figure 3), characterizing the dependence of the degree of radionuclide recovery on time. The analysis of curves showed that for each radionuclide under study the time of reaching the sorption equilibrium varies. In particular, for americium the equilibrium was established in 7 days, for cesium 10 days, in the case of strontium, within the margin of error ( $\pm 5\%$ ), we can assume 10–11 days. Surface distribution coefficients ( $K_a$ ) of Cs-137, Sr-90 and Am-241 calculated on the disc surface area were 6.6, 0.9 and 26.1 (mL cm<sup>-2</sup>), respectively. Thus, the sorption capacity of the studied sample R-11 in relation to radionuclides increases in the series Sr-90 < Cs-137 < Am-241, where americium is the most retained radionuclide in this sample. Based on the data on the distribution coefficients, it was possible to establish the general sorption capacity of the sample, while the sample itself is rather heterogeneous and is represented by a number of mineral phases with different sorption capacities.

**Figure 3.** Kinetics of Cs, Sr and Am sorption on the discs of sample R-11.

### 3.3. Spatial Microdistribution of Radionuclides on the Surface of Discs of Sample R-11

To study the behavior of Cs-137, Sr-90 and Am-241 on the whole sample R-11, black-and-white images of radiograms of three corresponding discs after sorption experiments were obtained (Figures 4 and 5). The darkened areas of the radiograms correspond to the places of radionuclide localization. It was found that Cs-137 and Sr-90 radionuclides are distributed extremely nonuniformly over the sample surface; these radionuclides were predominantly sorbed onto the secondary mineral chlorite. Americium sorbed with very similar efficiency on all mineral phases; only quartz and calcite have lower efficiency, as confirmed by the elemental maps (Figure 4).

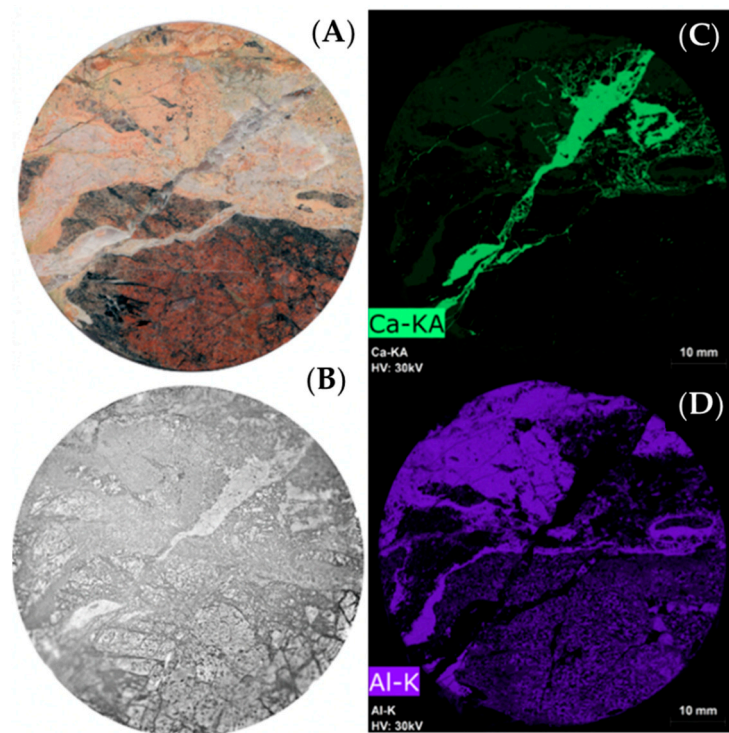


**Figure 4.** (A) optical image of sample R-11(disc (3)); (B) radiogram of americium sorption on sample R-11 (disc (3)); (C) elemental map of Ca distribution on the surface of R-11 sample (calcite identifying); (D) elemental map of Al distribution on the surface of R-11 sample (identifying of chlorite, epidote, feldspars, zeolite).

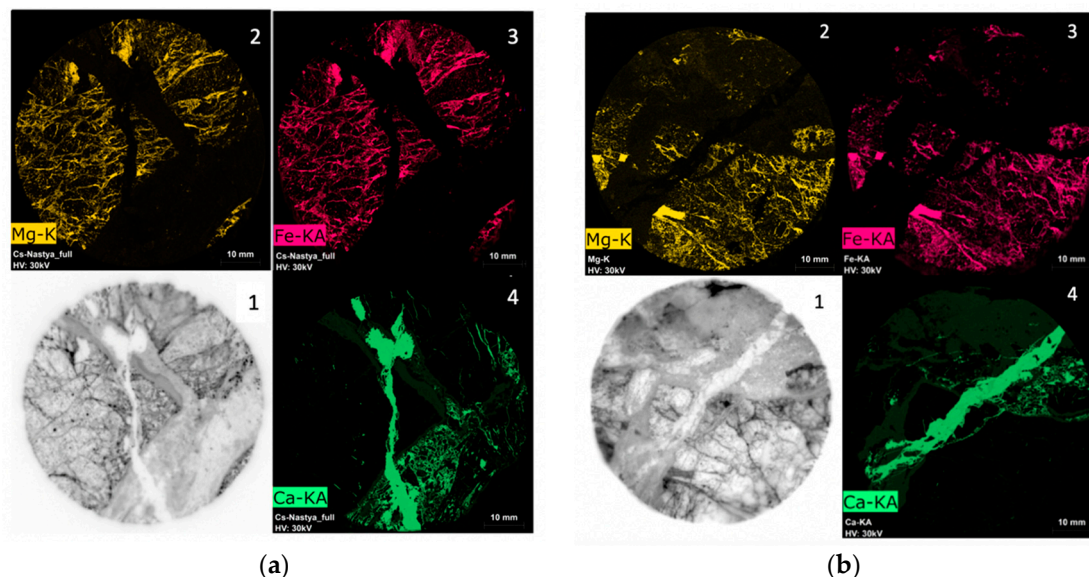


**Figure 5.** 1: radiograms of cesium (a) and strontium (b) sorption on the sample R-11 (disc 1 and 2, respectively); 2, 3: elemental maps of Mg and Fe distribution on the surface of R-11 sample (chlorite identifying); 4: elemental map of Ca distribution (calcite identifying).

The uniform distribution of americium on mineral phases of the whole sample R-11 (disc (3)) can be explained by its high sorption activity towards many mineral phases. It was noted that americium is well sorbed on all present mineral phases with distribution coefficient  $K_d \geq 10^3 \text{ mL g}^{-1}$ , and in some cases  $10^6 \text{ mL g}^{-1}$  [27–30]. For the mineral phases represented by carbonates (calcite), phosphates (apatite) and phyllosilicates (chlorite, biotite and muscovite),  $K_d$  values at pH 7 are  $10^4 \text{ mL g}^{-1}$ , which is an order higher than for



tectosilicates (quartz and feldspars). The mechanism of americium sorption on the studied mineral phases is a surface complex formation.

Chlorite, which belongs to the group of phyllosilicates, is the most effective sorbent for cesium (Figure 5). Zeolite has an average sorption capacity towards cesium, other mineral phases did not have a sufficient influence on cesium sorption, especially calcite, which has the lowest sorption activity (Figure 5). Due to a large ionic radius of cesium and a low charge, the mechanism of its sorption is an ionic exchange [31]. In a number of works, it was noted that a high sorption capacity in relation to cesium is typical for phyllosilicates ( $K_d \sim 10^3\text{--}10^4 \text{ mL g}^{-1}$ ). This can be explained by the presence of frayed edge sites that are most selective to cesium sorption in addition to a high cation exchange capacity caused by a crystallographic sheet structure [31–33]. The presence of exchangeable ions in the zeolite structure affects its sorption capacity with respect to cesium. Moreover, in a number of works, it was noted that zeolites have a sufficiently high cation exchange capacity [34,35]. As a result, the combination of two factors (the structure and the cation exchange capacity of zeolites) leads to a rather high sorption capacity of zeolites, and  $K_d$  values for cesium can reach  $10^4 \text{ mL g}^{-1}$  [36]. Other mineral phases such as quartz, feldspars and calcite are characterized by a low specific surface area and cation exchange capacity; therefore, a high efficiency of cesium sorption ( $K_d 10^2 \text{ mL g}^{-1}$ ) is not typical for them [31,33].

The strontium distribution over the mineral phases of the sample repeats the behavior of cesium (Figure 5). Strontium is well sorbed on chlorite, less on zeolite and the worst on calcite. Such similar behavior of strontium and cesium can be explained by a similar mechanism of strontium sorption on mineral phases, although in a number of works, in addition to ion exchange, the authors note the possibility of the formation of complexes on the mineral surface [37–39]. The sorption of strontium on phyllosilicates and zeolite is characterized by sufficiently high distribution coefficients ( $K_d \sim 10^3 \text{ mL g}^{-1}$ ) and is explained by the structure of minerals possessing ion exchange properties [36,40,41]. In comparison with phyllosilicates, calcite has a low strontium sorption efficiency ( $K_d \sim 10^2 \text{ mL g}^{-1}$ ), because strontium can form carbonate compounds, which are weakly sorbed by the calcite surface [42,43].

In addition to radiograms characterizing the distribution of cesium and strontium radionuclides, Figure 5 shows elemental maps of the elements magnesium and iron, which are part of the most effective phase of sorption (chlorite ( $\text{Fe}^{2+}$ , Mg, Al,  $\text{Fe}^{3+}$ ) $_6(\text{Si,Al})_4\text{O}_{10}(\text{OH},\text{O})_8$ ), and calcium, which is part of the less effective phase (calcite ( $\text{CaCO}_3$ )).

The separate strongly darkened areas of radiograms, in which the greatest localization of radionuclides occurred, were studied in detail by SEM-EDX analysis. As a result, it was confirmed that Cs-137 and Sr-90 radionuclides were predominantly sorbed in the cracks formed by chlorite, as well as in the fractured zones with mineral association (zeolite, chlorite and REE-silicates) (Figure 6a).

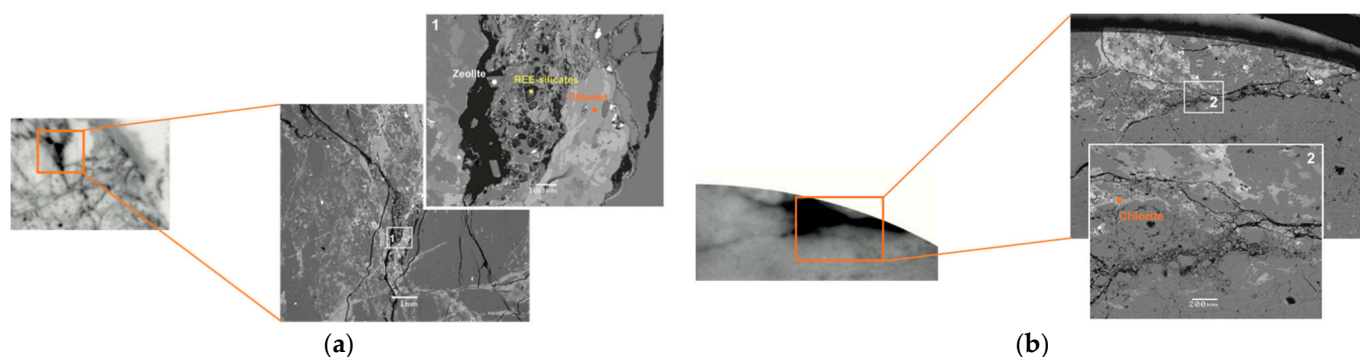


**Figure 6.** Cesium (a) and strontium (b) distribution in the fracture zone of R-11 sample (radiogram on the left, SEM images on the right); Chl—chlorite phase (the main filler of cracks).

In addition to the qualitative assessment of the distribution of the studied radionuclides, a quantitative assessment of the sorption of Cs-137, Sr-90 and Am-241 on the

fractured sample R-11 was established. Based on the previously developed methods [21,24], the parameters of the relative sorption efficiency (RSE) was determined (Figure 7).

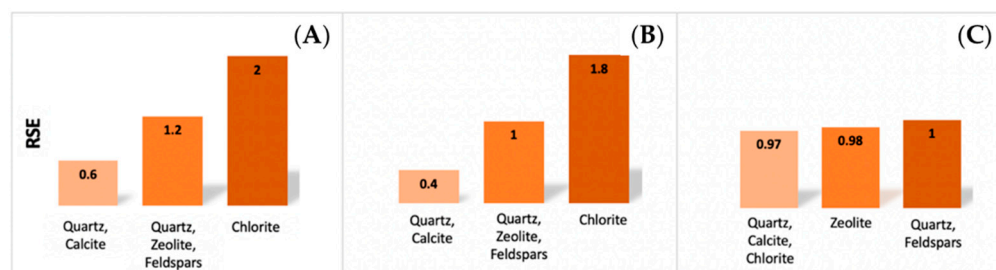


**Figure 7.** Relative sorption efficiency values of cesium (A), strontium (B) and americium (C) on mineral phases of R-11 sample.

It is important to specify that, for Cs-137 and Sr-90, the RSE was calculated based on the method using the ImageJ software. For Am-241, the semi-automatic procedure was the most suitable method, since the photo-stimulated luminescence (PSL) intensity for all mineral phases was approximately the same, so it was only possible to separate the mineral phases by an overlay of the optical image (ENVI program) on the radiogram. The data obtained agrees with earlier conclusions about radionuclide behavior: Am-241 is uniformly distributed on all mineral phases and the RSE values vary from 0.97 to 1, whereas for Cs-137 and Sr-90 the most effective retaining phase is chlorite, with RSE equal to 2 and 1.8, respectively (Figure 8). However, it was not possible to determine the RSE for each mineral in the system, because, firstly, some phases form mineral associations (quartz, feldspars and zeolite), and, secondly, for some minerals, the PSL values are the same. For such cases, general values on the RSE are provided.

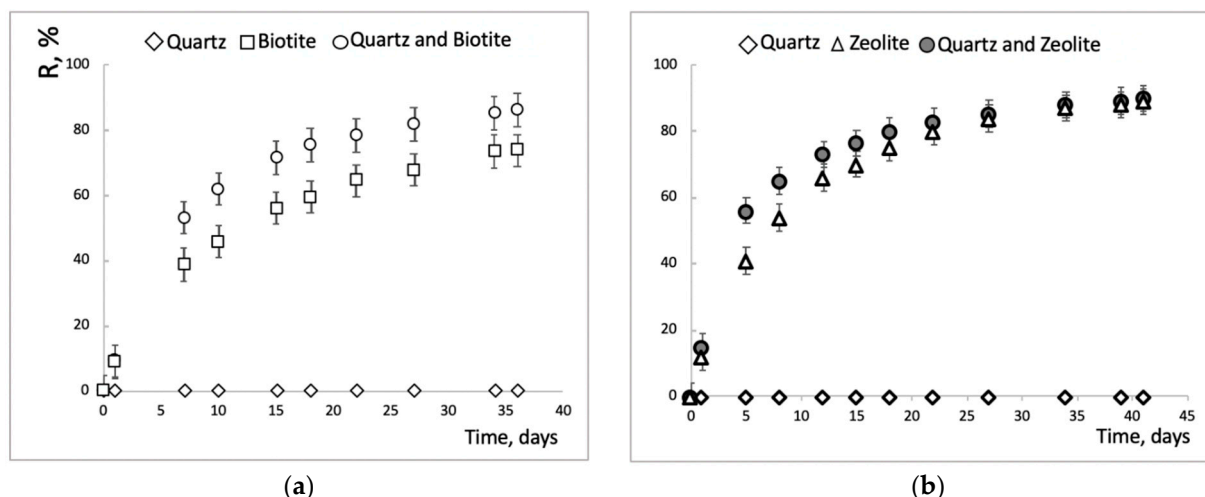


**Figure 8.** Kinetic of cesium sorption on crushed mineral phases (a) quartz, biotite phases in different containers (monomineral sorption), quartz and biotite in the same container (competitive sorption); (b) quartz, zeolite NaA in different containers (monomineral sorption), quartz and zeolite NaA in the same container (competitive sorption).

### 3.4. Sorption Experiments on Crushed Minerals, Imitating the Mineral Phases of Fractured sample R-11

The next stage of work was to study cesium behavior on the crushed mineral phases of quartz, biotite and zeolite NaA which were presented both by individual minerals in separated containers and by individual minerals in the same container (competitive sorption). The minerals were grouped into quartz–biotite and quartz–zeolite NaA (Figure S1) systems. The achievement of sorption equilibrium was determined by the kinetic sorption curves presented in Figure 8. The distribution coefficients of cesium for the mineral phases

of quartz, biotite and zeolite NaA were determined by measuring the activity of sorbed cesium on the powders of these minerals after their separation from the solutions (Table 3). It is shown that cesium sorption in the heterogeneous system of the two mineral phases biotite and quartz proceeds more effectively than the total sorption of the same mineral phases separately (Figure 8a). In case of the zeolite–quartz system, the difference between the total sorption of the separate minerals and the sorption in the heterogeneous system differs insignificantly (Figure 8b). According to the obtained values of the distribution coefficients (Table 3), it can be noted that the sorption of cesium on zeolite NaA is more effective than on biotite; explained by a greater specific surface of synthetic zeolite NaA in comparison with natural biotite.

**Table 3.** Cesium distribution coefficients on mineral phases in the cases of monomineral sorption and competitive sorption between quartz and biotite, quartz and zeolite NaA. RSE parameters determined in the case of competitive sorption of the same minerals.

| System | Minerals | $K_d, \text{mL g}^{-1}$ |                      | RSE |
|--------|----------|-------------------------|----------------------|-----|
|        |          | Monomineral Sorption    | Competitive Sorption |     |
| a      | quartz   | 3.2                     | 2.5                  | 0.2 |
|        | biotite  | $1.2 \cdot 10^3$        | $2.7 \times 10^3$    | 1.1 |
| b      | quartz   | 3.2                     | 1.5                  | 0.1 |
|        | zeolite  | $4.4 \cdot 10^3$        | $4.6 \times 10^3$    | 1.0 |

To interpret the values of cesium RSE on mineral phases of the whole sample R-11 (Figure 7a), we determined the values of cesium RSE for minerals in the quartz–biotite (a) and quartz–zeolite (b) systems (Table 3). Comparing the ratios of RSE values of cesium between the highly sorbing mineral phases (biotite (Table 3), chlorite (Figure 7)) and poorly sorbing ones (quartz (Table 3)), and the association of quartz/calcite (Figure 7) from various experiments, we should note a significant difference. In the case of the quartz–biotite system, where the mineral phases are represented by powders (Table 3), the RSE values of cesium differ 5.5 times. In the case of the RSE values of cesium on the minerals of the whole sample R-11 (Figure 7), the values between chlorite and the association of quartz/calcite differ 3.3 times. Such a significant difference can be explained by the different surface of the represented mineral phases, because, for the whole sample, the surface of the mineral phases was calculated from the geometric size without taking into account the porosity and the specific surface of the powders was determined by the BET method. Moreover, in [44], the authors noted that, during the crushing of the minerals, additional sorption centers are formed due to the appearance of an internal specific surface, thus contributing to the radionuclide sorption.

### 3.5. Modeling of Cesium, Strontium and Americium Sorption on the Fractured Rock Sample

As a result of the sorption experiments on the whole fractured sample R-11, the sorption of Cs-137, Sr-90 and Am-241 in this sample was modeled. Table 2 shows the areas occupied by the different minerals on the surface of the polished sample. It was assumed that the sorption of cesium, strontium and americium on the surface of the polished sample is primarily caused by a radionuclide interaction with chlorite. The density of chlorite was assumed to be  $2.75 \text{ g cm}^{-3}$  [45]. The initial activities of Cs-137, Sr-90 and Am-241 in the aqueous solution were 430, 285 and  $15 \text{ Bq mL}^{-1}$ , respectively (or  $9.753 \times 10^{-10}$ ,  $6.27 \times 10^{-10}$  and  $4.90 \times 10^{-10} \text{ mol L}^{-1}$ ).

#### 3.5.1. Modeling of Cesium Sorption

Cesium sorption on the surface of the fractured sample R-11 was simulated using the model of the cesium and montmorillonite sorption interaction proposed in [46]. This model assumes that the cesium sorption from an aqueous solution occurs on the mineral surface via the ion exchange mechanism and appears in three structural positions: (1) planar sites,

(2) type II sites and (3) frayed edge sites. Each structural position is distinguished by a set of competing for ion exchange reactions with varying ion exchange capacities (normalized to the mass of the sorbent) (Table 4).

**Table 4.** Ion exchange reactions and selectivity coefficients ( $K_c$ ) at “planar sites”, “type II sites” and “frayed edge sites” (data from [46]).

| Ion Exchange Reaction                          | $\lg K_c$ | Cation Exchange Capacity, meq kg <sup>-1</sup> |
|--|-----------|--|
| Planar Sites (PS)                              |           |  |
| Cs <sup>+</sup> + KX = CsX + K <sup>+</sup>    | 0.5       | 160  |
| Cs <sup>+</sup> + NaXb = CsX + Na <sup>+</sup> | 1.6       |  |
| K <sup>+</sup> + NaX = KX + Na <sup>+</sup>    | 1.1       |  |
| Type II sites                                  |           |  |
| Cs <sup>+</sup> + KX = CsX + K <sup>+</sup>    | 1.5       | 40   |
| Cs <sup>+</sup> + NaX = CsX + Na <sup>+</sup>  | 3.6       |  |
| K <sup>+</sup> + NaX = KX + Na <sup>+</sup>    | 2.1       |  |
| Frayed Edge Sites                              |           |  |
| Cs <sup>+</sup> + KX = CsX + K <sup>+</sup>    | 4.6       | 0.5  |
| Cs <sup>+</sup> + NaX = CsX + Na <sup>+</sup>  | 7.0       |  |
| K <sup>+</sup> + NaX = KX + Na <sup>+</sup>    | 2.4       |  |

The ion exchange capacity value was multiplied by the mass of chlorite in contact with the aqueous solution to estimate the amount of chlorite ion exchange positions in equilibrium with the aqueous solution. The chlorite mass was calculated as the product of chlorite density, its area on the surface of the polished plate, and the depth of the aqueous solution penetration inside the sample. The depth of the aqueous solution penetration was estimated by fitting it in such a way that the modeled estimates of dissolved cesium content after the sorption experiment agreed with the experimentally obtained value.

According to the modeling, the depth of the aqueous solution penetration should be set to 0.11 mm in order to achieve agreement between the experimentally obtained values of dissolved cesium after the sorption experiment. In other words, during the sorption experiment, 0.01 g of chlorite reacted with the solution.

### 3.5.2. Modeling of Strontium Sorption

To simulate the strontium sorption on chlorite, a combined model including ion exchange reactions and surface complexation reactions on the illite surface [47] was used (Table 5).

The depth of the aqueous solution penetration was assumed to be 0.11 mm based on the results of the simulation of cesium sorption on the surface of the polished sample. Thus, 0.01 g of chlorite was assumed to react with the aqueous solution to simulate the strontium sorption on the sample surface.

However, modeling has shown that this amount of chlorite is insufficient to sorb the required amount of strontium from the aqueous solution and to obtain the agreement between the experimentally obtained and modeled concentrations of strontium in an aqueous solution. The model estimate of dissolved strontium concentration ( $6.195 \times 10^{-10} \text{ mol L}^{-1}$  or 281.4 Bq ml<sup>−1</sup>) is significantly higher than the experimentally determined value ( $2.202 \times 10^{-10} \text{ mol L}^{-1}$  or 100 Bq ml<sup>−1</sup>). The penetration depth of the aqueous solution into the polished sample should be 0.25 mm in order to achieve agreement between the model and the experimental results on the Sr-90 activities in the solution.

### 3.5.3. Modeling of Americium Sorption

The model [48] implying sorption at strong and weak sites as well as ion exchange reactions was used to simulate the sorption of americium on a polished rock sample. Table 6 displays the model parameters.



**Table 5.** The model parameters used for the simulation of the Sr-90 sorption on the polished sample (data from [47]).

| Surface Complexation Sites   | Site Densities                           |
|--|--|
| $\equiv\text{S}^{\text{S}}\text{OH}$   | $2 \times 10^{-3} \text{ mol kg}^{-1}$   |
| $\equiv\text{S}^{\text{W1}}\text{OH}$  | $4.5 \times 10^{-2} \text{ mol kg}^{-1}$ |
| $\equiv\text{S}^{\text{W2}}\text{OH}$  | $4.5 \times 10^{-2} \text{ mol kg}^{-1}$ |
| Ion Exchange Sites   | Cation Exchange Capacity                 |
| $\text{X}^{-}$   | $200 \text{ meq kg}^{-1}$                |
| Protonation/Deprotonation Reactions  | $\log_{10}K$                             |
| $\equiv\text{S}^{\text{S}}\text{OH} + \text{H}^{+} = \equiv\text{S}^{\text{S}}\text{OH}_2^{+}$                   | 5.5                                      |
| $\equiv\text{S}^{\text{S}}\text{OH} = \equiv\text{S}^{\text{S}}\text{O}^{-} + \text{H}^{+}$                      | −6.2                                     |
| $\equiv\text{S}^{\text{W1}}\text{OH} + \text{H}^{+} = \equiv\text{S}^{\text{W1}}\text{OH}_2^{+}$                 | 5.5                                      |
| $\equiv\text{S}^{\text{W1}}\text{OH} = \equiv\text{S}^{\text{W1}}\text{O}^{-} + \text{H}^{+}$                    | −6.2                                     |
| $\equiv\text{S}^{\text{W2}}\text{OH} + \text{H}^{+} = \equiv\text{S}^{\text{W2}}\text{OH}_2^{+}$                 | 9.0                                      |
| $\equiv\text{S}^{\text{W2}}\text{OH} = \equiv\text{S}^{\text{W2}}\text{O}^{-} + \text{H}^{+}$                    | −10.5                                    |
| Ion Exchange Reactions   | $\log_{10}K$                             |
| $2\text{NaX} + \text{Sr}^{2+} = \text{SrX}_2 + 2\text{Na}^{+}$   | 1.04                                     |
| $3\text{NaX} + \text{Al}^{3+} = \text{AlX}_3 + 3\text{Na}^{+}$   | 1.00                                     |
| Surface Complexation Reactions   | $\log_{10}K$                             |
| $\equiv\text{S}^{\text{W2}}\text{OH} + \text{Sr}^{2+} = \equiv\text{S}^{\text{W2}}\text{OSr}^{+} + \text{H}^{+}$ | −5.00                                    |

**Table 6.** The model parameters used for the simulation of the Am-241 sorption on the polished sample (data from [48]).

| Site Surface   | Site Density, $\text{mol kg}^{-1}$ |
|--|------------------------------------|
| $\equiv\text{S}^{\text{S}}\text{OH}$   | $2.0 \times 10^{-3}$               |
| $\equiv\text{S}^{\text{W1}}\text{OH}$  | $4.0 \times 10^{-2}$               |
| $\equiv\text{S}^{\text{W2}}\text{OH}$  | $4.0 \times 10^{-2}$               |
| Cation Exchange Capacity, $\text{meq kg}^{-1}$   | $8.7 \times 10^{-1}$               |
| Protonation/Deprotonation Reactions  | $\log_{10}K$                       |
| $\equiv\text{S}^{\text{S}}\text{OH} + \text{H}^{+} = \equiv\text{S}^{\text{S}}\text{OH}_2^{+}$   | 4.5                                |
| $\equiv\text{S}^{\text{S}}\text{OH} = \equiv\text{S}^{\text{S}}\text{OH}_2^{+} + \text{H}^{+}$   | −7.9                               |
| $\equiv\text{S}^{\text{W1}}\text{OH} + \text{H}^{+} = \equiv\text{S}^{\text{W1}}\text{OH}_2^{+}$   | 4.5                                |
| $\equiv\text{S}^{\text{W1}}\text{OH} = \equiv\text{S}^{\text{W1}}\text{O}^{-} + \text{H}^{+}$  | −7.9                               |
| $\equiv\text{S}^{\text{W2}}\text{OH} + \text{H}^{+} = \equiv\text{S}^{\text{W2}}\text{OH}_2^{+}$   | 6.0                                |
| $\equiv\text{S}^{\text{W2}}\text{OH} = \equiv\text{S}^{\text{W2}}\text{O}^{-} + \text{H}^{+}$  | −10.5                              |
| Surface Complexation Reactions   | $\log_{10}K$                       |
| $\equiv\text{S}^{\text{S}}\text{OH} + \text{Am}^{3+} = \equiv\text{S}^{\text{S}}\text{OAm}^{2+} + \text{H}^{+}$                                    | 1.8                                |
| $\equiv\text{S}^{\text{S}}\text{OH} + \text{Am}^{3+} + \text{H}_2\text{O} = \equiv\text{S}^{\text{S}}\text{OAmOH}^{+} + 2\text{H}^{+}$             | −5.4                               |
| $\equiv\text{S}^{\text{S}}\text{OH} + \text{Am}^{3+} + 3\text{H}_2\text{O} = \equiv\text{S}^{\text{S}}\text{OAm}(\text{OH})_3^{-} + 4\text{H}^{+}$ | −22.1                              |
| $\equiv\text{S}^{\text{W1}}\text{OH} + \text{Am}^{3+} = \equiv\text{S}^{\text{W1}}\text{OAm}^{2+} + \text{H}^{+}$                                  | −0.5                               |
| Ion exchange reactions   | $\log_{10}K$                       |
| $\text{Am}^{3+} + 3\text{NaX} = \text{AmX}_3 + 3\text{Na}^{+}$   | 1.477                              |
| $\text{Am}^{3+} + 1.5\text{CaX}_2 = \text{AmX}_3 + 1.5\text{Ca}^{2+}$  | 1.283                              |

The calculations revealed that, in order to numerically reproduce the experimentally obtained results on americium activity in an aqueous solution, the aqueous solution must penetrate to a depth of 0.7 mm.

Thus, the results of the sorption experiments were numerically reproduced, assuming the radionuclide sorption models on illite–smectite minerals. The number of sorption

structural positions was adjusted in such a way that the results of the calculations best reproduced the experimental results. During modeling, it was assumed that chlorite is the most effective radionuclide phase sorbent. It was discovered that the number of sorption structural positions can be calculated by taking the chlorite area on the polished rock sample, its density and the depth of the radioactive solution penetration inside the rock into account.

The variability in the estimates of the depth of the solution penetration into the rock during the sorption of cesium, strontium and americium (0.11, 0.25 and 0.70 mm, respectively) can be attributed to the sample's significant heterogeneity due to its mineral composition and other properties (i.e., porosity). Thus, in order to clarify the obtained results of the diffusion parameters, it is necessary to conduct additional studies for other rock samples of the Nizhnekansky granitoid massif.

#### 4. Conclusions

The sorption properties of a whole sample of fractured rock from borehole R-11 of the Nizhnekansky granitoid massif in relation to Cs, Sr and Am were studied. It was noted that the sorption capacity of the studied sample with respect to radionuclides increases in the range  $Sr < Cs < Am$ , where americium is the most retained radionuclide. The distribution of Cs, Sr and Am on the mineral phases of the presented fractured sample was investigated by the method of digital autoradiography. As a result of the processing of digitized radiograms with SEM images, the RSE values were obtained, which allowed to quantitatively estimate the contribution of the mineral phases of the fractured sample in the sorption of radionuclides. On the basis of the data obtained for each radionuclide studied except americium, the most effective sorbing phases were established. It was shown that cesium and strontium are predominantly retained in cracks filled with secondary mineral chlorite. Zeolite is a less effective sorbent with respect to cesium and strontium. Americium was sorbed with close values of efficiency (RSE  $\sim 1$ ) on all mineral phases.

The quantitative contribution of mineral phases to the minerals of the fractured sample of the Nizhnekansky granitoid massif to cesium sorption has been estimated using the examples of crushed quartz, biotite and zeolite grouped into heterogeneous systems. It was shown that the cesium sorption in the heterogeneous system of the two-mineral phases, biotite and quartz, proceeds more effectively than the total sorption of the same mineral phases separately. There is a significant variation in the difference in the RSE values of cesium between highly sorbing mineral phases and poorly sorbing mineral phases in the system of the competitive sorption on crushed minerals and the system of minerals of a whole rock fractured sample of the Nizhnekansky granitoid massif. This difference may be due to the developed surface and the presence of additional sorption centers of crushed minerals compared with the surface of minerals, represented by a whole sample. Thus, the competitive sorption of radionuclides in the presence of two or more mineral phases is a complex process and should be studied more to provide further modeling of the migration behavior of radionuclides.

Based on the models of the cesium, strontium and americium sorption on illite-smectite minerals, the depths of the penetration of the solution containing radionuclide under study into the fractured rock sample of Nizhnekansky granitoid massif were estimated. The variable depths of the solution penetration into the rock sample were established, that is, they were attributed to the sample's significant heterogeneity due to its mineral composition and other properties (i.e., porosity).

**Supplementary Materials:** The following supporting information can be downloaded at: <https://www.mdpi.com/article/10.3390/en15197440/s1>, Figure S1: Scheme of sorption experiments on polished discs of fractured rock sample R-11; Figure S2: Sorption cesium on crushed quartz and biotite in separated containers and in the same container; Table S1: Composition of core sample from borehole R-11 (249 m) of «Yeniseysky» site; Table S2: Determination of mineral phases of a core sample R-11 by the micro XRF method.

**Author Contributions:** Conceptualization, V.G.P. and K.B.R.; methodology, V.G.P., A.A.R., I.E.V. and K.B.R.; validation, V.G.P., A.A.R., I.E.V. and K.B.R.; formal analysis, A.A.R., K.B.R., V.O.Y. and I.M.N.; investigation, A.A.R. and K.B.R.; resources, I.E.V.; writing—original draft preparation, A.A.R. and K.B.R.; writing—review and editing, V.G.P., I.E.V., I.M.N., V.G.R. and S.N.K.; visualization, V.G.P.; supervision, V.G.P., I.E.V., V.G.R. and S.N.K.; project administration, V.G.P.; funding acquisition, I.E.V. and A.A.R. All authors have read and agreed to the published version of the manuscript.

**Funding:** This work was financially supported by the Russian Science Foundation grant No. 19-73-20051 (in part for carrying out of sorption experiments) and state task of GEOKHI RAS (in part for preparing mineral samples).

**Conflicts of Interest:** The authors declare no conflict of interest.

## References

- McKinley, I.G.; Russell Alexander, W.; Blaser, P.C. Development of Geological Disposal Concepts. *Radioact. Environ.* **2007**, *9*, 41–76. [\[CrossRef\]](#)
- IAEA. *Geological Disposal Facilities for Radioactive Waste. Specific Safety Guide*; IAEA: Vienna, Austria, 2011; p. 124.
- NDA. *Geological Disposal, Generic Environmental Safety Case—Main Report*; NDA: Didcot, UK, 2016; p. 185.
- Pusch, R. *Geological Storage of Radioactive Waste*; Springer International Publishing: Berlin/Heidelberg, Germany, 2008; Volume 53, ISBN 9783540773320.
- Alexander, W.R.; Kickmaier, W.; Vomvoris, S.; Kaku, K.; McKinley, I.G. Nagra's grimsel URL: From underground testing to the demonstration of disposal systems. In Proceedings of the 10th International Conference on Environmental Remediation and Radioactive Waste Management ICEM'05 2005, Glasgow, Scotland, 4–8 September 2005; pp. 1678–1683.
- Hölttä, P. *Radionuclide Migration in Crystalline Rock Fractures. Academic Dissertation*; University of Helsinki: Helsinki, Finland, 2002; p. 55.
- Michael, B. *Stephens Forsmark Site Investigation. Bedrock Geology—Overview and Excursion Guide*; SKB Report; Svensk Kärnbränslehantering AB: Stockholm, Sweden, 2010; p. 52.
- Ota, K.; Abe, H.; Kunimaru, T. *Horonobe Underground Research Laboratory Project Synthesis of Phase I Investigations 2001–2005, Volume “Geoscientific Research”*; JAEA: Ibaraki-Ken, Japan, 2011.
- Laverov, N.P.; Yudin, S.V.; Kochkin, B.T.; Malkovsky, V.I. The Russian Strategy of Using Crystalline Rock as a Repository for Nuclear Waste. *Elements* **2016**, *12*, 253–256. [\[CrossRef\]](#)
- Jardin, L.J.; Gupalo, T.A. *Development of a Comprehensive Plan for Scientific Research, Exploration, and Design: Creation of an Underground Radioactive Waste Isolation Facility at the Nizhnekansky Rock Massif*; ISTC: Moscow, Russia, 2005; p. 474.
- Igin, V.; Krasilnikov, V. Creation of System of Final Isolation (Disposal) of Radioactive Waste in the Russian Federation. *Mrs Adv.* **2020**, *5*, 275–282. [\[CrossRef\]](#)
- Gupalo, V.S. Spatial Characterization of the Physical Process Parameters in Rock Mass during Construction of the Underground Facility for the RW Disposal. *Russ. J. Earth Sci.* **2019**, *19*, 670. [\[CrossRef\]](#)
- Mahmoudzadeh, B.; Liu, L.; Moreno, L.; Neretnieks, I. Solute Transport in Fractured Rocks with Stagnant Water Zone and Rock Matrix Composed of Different Geological Layers-Model Development and Simulations. *Water Resour. Res.* **2013**, *49*, 1709–1727. [\[CrossRef\]](#)
- Cvetkovic, V.; Cheng, H.; Widestrand, H.; Byegård, J.; Winberg, A.; Andersson, P. Sorbing Tracer Experiments in a Crystalline Rock Fracture at Äspö (Sweden): 2. Transport Model and Effective Parameter Estimation. *Water Resour. Res.* **2007**, *43*, 1–16. [\[CrossRef\]](#)
- Neretnieks, I. Channeling with Diffusion into Stagnant Water and into a Matrix in Series. *Water Resour. Res.* **2006**, *42*, 1–15. [\[CrossRef\]](#)
- Vandergaaf, T.T.; Drew, D.J.; Archambault, D.; Ticknor, K.V. Transport of Radionuclides in Natural Fractures: Some Aspects of Laboratory Migration Experiments. *J. Contam. Hydrol.* **1997**, *26*, 83–95. [\[CrossRef\]](#)
- Hu, Q.H.; Möri, A. Radionuclide Transport in Fractured Granite Interface Zones. *Phys. Chem. Earth* **2008**, *33*, 1042–1049. [\[CrossRef\]](#)
- Rozov, K.B.; Rumynin, V.G.; Nikulenkov, A.M.; Leskova, P.G. Sorption of  $^{137}\text{Cs}$ ,  $^{90}\text{Sr}$ ,  $^{99}\text{Tc}$ ,  $^{152(154)}\text{Eu}$ ,  $^{239(240)}\text{Pu}$  on Fractured Rocks of the Yeniseysky Site (Nizhne-Kansky Massif, Krasnoyarsk Region, Russia). *J. Environ. Radioact.* **2018**, *192*, 513–523. [\[CrossRef\]](#)
- Metcalfe, R.; Milodowski, A.E.; Field, L.P.; Wogelius, R.A.; Carpenter, G.; Yardley, B.W.D.; Norris, S. Natural Analogue Evidence for Controls on Radionuclide Uptake by Fractured Crystalline Rock. *Appl. Geochem.* **2021**, *124*, 104812. [\[CrossRef\]](#)

20. Ticknor, K.V.; Vandergraaf, T.T.; Kamineni, D.C. Radionuclide Sorption on Primary and Fracture-Filling Minerals from the East Bull Lake Pluton, Massey, Ontario, Canada. *Appl. Geochem.* **1989**, *4*, 163–176. [\[CrossRef\]](#)
21. Petrov, V.G.; Vlasova, I.E.; Rodionova, A.A.; Yapaskurt, V.O.; Korolev, V.V.; Petrov, V.A.; Poluektov, V.V.; Hammer, J.; Kalmykov, S.N. Preferential Sorption of Radionuclides on Different Mineral Phases Typical for Host Rocks at the Site of the Future Russian High Level Waste Repository. *Appl. Geochem.* **2019**, *100*, 90–95. [\[CrossRef\]](#)
22. ENVI. *ENVI User's Guide Restricted Rights Notice*; ENVI: Broomfield, CO, USA, 2009.
23. Zhang, M.; Chen, Q.; Li, X.-F.; O'Donoghue, J.; Ruan, S.; Zanzonico, P.; Ling, C.C.; Humm, J.L. Image Deconvolution in Digital Autoradiography: A Preliminary Study. *Med. Phys.* **2008**, *35*, 522–530. [\[CrossRef\]](#)
24. Rodionova, A.A.; Petrov, V.G.; Vlasova, I.E.; Yapaskurt, V.O.; Petrov, V.A.; Poluektov, V.V.; Hammer, J.; Kalmykov, S.N. Digital Radiography for Evaluating the Relative Efficiency of Radionuclide Sorption onto Various Rock Minerals. *Radiochemistry* **2019**, *61*, 37–43. [\[CrossRef\]](#)
25. ImageJ User Guide. Available online: <http://imagej.nih.gov/ij/docs/guide/user-guide.pdf> (accessed on 25 August 2022).
26. Parkhurst, D.L.; Appelo, C.A.J. *Description of Input and Examples for PHREEQC Version 3—A Computer Program for Speciation, Batch-Reaction, One-Dimensional Transport, and Inverse Geochemical Calculations*; Book 6, Chap. A43; US Geological Survey: Lakewood, CO, USA, 2013; p. 497.
27. Allard, B.; Beall, G.W. Sorption of Americium on Geologic Media. *J. Environ. Sci. Health Part A Environ. Sci. Eng.* **1979**, *14*, 507–518. [\[CrossRef\]](#)
28. Moulin, V.; Stammose, D. Effect of Humic Substances on Americium (III) Retention onto Silica. *MRS Proc.* **1988**, *127*, 723. [\[CrossRef\]](#)
29. Fröhlich, D.R.; Kaplan, U. Sorption of Am(III) on Clays and Clay Minerals: A Review. *J. Radioanal. Nucl. Chem.* **2018**, *318*, 1785–1795. [\[CrossRef\]](#)
30. Wang, P.; Anderko, A.; Turner, D.R. Thermodynamic Modeling of the Adsorption of Radionuclides on Selected Minerals. I: Cations. *Ind. Eng. Chem. Res.* **2001**, *40*, 4428–4443. [\[CrossRef\]](#)
31. Cornell, R.M. Adsorption of Cesium on Minerals: A Review. *J. Radioanal. Nucl. Chem. Artic.* **1993**, *171*, 483–500. [\[CrossRef\]](#)
32. McKinley, J.P.; Zachara, J.M.; Heald, S.M.; Dohnalkova, A.; Newville, M.G.; Sutton, S.R. Microscale Distribution of Cesium Sorbed to Biotite and Muscovite. *Environ. Sci. Technol.* **2004**, *38*, 1017–1023. [\[CrossRef\]](#) [\[PubMed\]](#)
33. Muuri, E.; Ikonen, J.; Matara-aho, M.; Lindberg, A.; Holgersson, S.; Voutilainen, M.; Siitari-Kauppi, M.; Martin, A. Behavior of Cs in Grimsel Granodiorite: Sorption on Main Minerals and Crushed Rock. *Radiochim. Acta* **2016**, *104*, 575–582. [\[CrossRef\]](#)
34. Baek, W.; Ha, S.; Hong, S.; Kim, S.; Kim, Y. Cation Exchange of Cesium and Cation Selectivity of Natural Zeolites: Chabazite, Stilbite, and Heulandite. *Microporous Mesoporous Mater.* **2018**, *264*, 159–166. [\[CrossRef\]](#)
35. Rajec, P.; Mátel, L.; Orechovská, J.; Šúcha, J.; Novák, I. Sorption of Radionuclides on Inorganic Sorbents. *J. Radioanal. Nucl. Chem.* **1996**, *208*, 477–486. [\[CrossRef\]](#)
36. Elizondo, N.V.; Ballesteros, E.; Kharisov, B.I. Cleaning of Liquid Radioactive Wastes Using Natural Zeolites. *Appl. Radiat. Isot.* **2000**, *52*, 27–30. [\[CrossRef\]](#)
37. Smičiklas, I.; Dimović, S.; Plečaš, I. Removal of Cs<sup>1+</sup>, Sr<sup>2+</sup> and Co<sup>2+</sup> from Aqueous Solutions by Adsorption on Natural Clinoptilolite. *Appl. Clay Sci.* **2007**, *35*, 139–144. [\[CrossRef\]](#)
38. Hu, B.; Hu, Q.; Xu, D.; Chen, C. Macroscopic and Microscopic Investigation on Adsorption of Sr(II) on Sericite. *J. Mol. Liq.* **2017**, *225*, 563–568. [\[CrossRef\]](#)
39. Lee, S.S.; Fenter, P.; Park, C.; Sturchio, N.C.; Nagy, K.L. Hydrated Cation Speciation at the Muscovite (001)-Water Interface. *Langmuir* **2010**, *26*, 16647–16651. [\[CrossRef\]](#)
40. Söderlund, M.; Ervanne, H.; Muuri, E.; Lehto, J. The Sorption of Alkaline Earth Metals on Biotite. *Geochem. J.* **2019**, *53*, 223–234. [\[CrossRef\]](#)
41. Marinin, D.V.; Brown, G.N. Studies of Sorbent/Ion-Exchange Materials for the Removal of Radioactive Strontium from Liquid Radioactive Waste and High Hardness Groundwaters. *Waste Manag.* **2000**, *20*, 545–553. [\[CrossRef\]](#)
42. Bellenger, J.P.; Staunton, S. Adsorption and Desorption of <sup>85</sup>Sr and <sup>137</sup>Cs on Reference Minerals, with and without Inorganic and Organic Surface Coatings. *J. Environ. Radioact.* **2008**, *99*, 831–840. [\[CrossRef\]](#) [\[PubMed\]](#)
43. Zachara, J.M.; Cowan, C.E.; Resch, C.T. Sorption of Divalent Metals on Calcite. *Geochim. Cosmochim. Acta* **1991**, *55*, 1549–1562. [\[CrossRef\]](#)
44. Lehto, J.; Puukko, E.; Lindberg, A.; Voutilainen, M. Batch Sorption Experiments of Cesium and Strontium on Crushed Rock and Biotite for the Estimation of Distribution Coefficients on Intact Crystalline Rock. *Heliyon* **2019**, *5*, e02296. [\[CrossRef\]](#) [\[PubMed\]](#)
45. Godovikov, A.A. *Mineralogy*, 2nd ed.; Revised and Enlarged; Nedra: Moscow, Russia, 1983.
46. Bradbury, M.H.; Baeyens, B. A Generalised Sorption Model for the Concentration Dependent Uptake of Caesium by Argillaceous Rocks. *J. Contam. Hydrol.* **2000**, *42*, 141–163. [\[CrossRef\]](#)
47. Bradbury, M.H.; Baeyens, B. *Experimental and Modelling Investigations on Na-Illite: Acid-Base Behavior and the Sorption of Strontium, Nickel, Europium and Uranyl*; Paul Scherrer Institute: Villigen, Switzerland, 2005.
48. Bradbury, M.; Baeyens, B. Sorption of Eu on Na- and Ca-Montmorillonites: Experimental Investigations and Modelling with Cation Exchange and Surface Complexation. *Geochim. Cosmochim. Acta* **2002**, *66*, 2325–2334. [\[CrossRef\]](#)